1.1. Introduction

The development of modern technology based on multifunctional materials is showing the path to new applications for technological challenges like data storage, spintronic, sensor, actuator etc [Eerenstein et al. (2006); Wang et al. (2009)]. Multiferroic materials have experienced a resurgence of interest after the discovery in 2003-2004 of compounds that display large cross-coupling effects between magnetic and ferroelectric order parameters in $TbMnO_3$,$TbMn_2O_5$, $HoMnO_3$ etc.[Kimura et al. (2003), Hur et al. (2004) and Lottermoser et al. (2004)]. Particular interest aroused by the possibility of new magnetoelectric coupling mechanisms like electric polarization can be induced at domain walls and that magnetic vortices carry electric charge, whereas in another case, magnetism can drive ferroelectricity without breaking the inversion symmetry of the magnetic ordering [Mostovoy (2006), Betouras et al. (2007) and Cheong et al. (2007)] and its potential for technological applications [Fiebig (2005), Tokura (2006) and Eerenstein et al. (2006)]. Amongst the magnetoelectric mutiferroic compounds, $BiFeO_3$ (BF) is the only room temperature multiferroic with very high ferroelectric (FE) and antiferromagnetic (AFM) transition temperatures of T_C = 1103 K and T_N = 643 K, respectively [Eerenstein et al. (2006), Fiebig et al. (2005)]. This material therefore holds considerable promise for multifunctional devices operating at room temperature [Fiebig et al. (2005), Eerenstein et al. (2006),Cheong et al.(2007)]. Solid solutions of BF with other pervoskite oxides have received considerable attention from the point of view of melting of the spin cycloid of BF Solid solution formation with other ABO_3 perovskites is known to destroy the spin cycloid due to introduction of disorder in the Fe^{3+}sublattice [Singh et al. (2008), (2012), Bhattacharjee et al. (2007), (2010), Patel et al. (2013)]. In this context, the solid solutions of BF with FE perovskite like $BaTiO_3$ (BT) and $PbTiO_3$ (PT)

have attracted much attention not only because of their weakly ferromagnetic behavior but also due to the emergence of new types of phase transitions like tricritical transition, morphotropic phase transition, isostructural ferroelectric to ferroelectric transition, critical end point, spin reorientation transition and spin glass transition [Singh et al. (2011), Bhattacharjee et al.(2011), (2013), Zhu et al. (2008)]. $PbTiO_3$ based solid solutions also display interesting meta properties like negative, near zero and positive thermal expansion in the same material in different temperature range [Bhattacharjee et al. (2011), Chen et al. (2013)]. Similarly, the $BaTiO_3$ based solid solutions are emerging as potential high temperature piezoelectric because of their extremely high depoling temperatures compared to existing piezoelectric ceramic materials [Lee et al. (2015), Hojo et al. (2018)]. It has been shown that the weak FM component of the canted spins of BF can also be recovered on reducing the size below 62 nm as a result of destruction of the spin cycloid [Park et al. (2007)]. The recovery of latent FM magnetization has been confirmed in nanocrystalline BF solid solutions [Park et al. (2010)]. The finite size affects the phase transition also as is well known in the context of ferroelectric, magnetic and superconducting transitions where size reduction below a critical value reduces the transition temperature (T_c) as per the predictions of the scaling theories [Ishikawa et al. (1988), Bose et al.(2014), Hojo et al. (2018)].

The present thesis deals with a comprehensive study of synthesis, crystal structures, magnetic properties and nature of ferroic transitions in nano-particles of (1- x)$BiFeO_3$-x$PbTiO_3$ (BF-xPT) solid solutions, whose one end member ($BiFeO_3$) is one of the most important multiferroic material; while the other one ($PbTiO_3$) is a ferroelectric material. Before, describing the details our investigations, we will briefly introduce some basic terms and the relevant ideas in this chapter. Subsequently, we will try to summarize the

results on the structure and multiferroic properties of pure $BiFeO_3$ as well as compositionally modified-$BiFeO_3$.

1.2 Ferroic ordering

The word ferroics is derived from "ferrum", a Latin word which means "iron" is the oldest known ferroic material. It is the most important class of materials with having unique properties which make it a leading candidate in the modern technologies such as data storage, electronics and sensor devices. A common feature observe by ferroic materials is their ability to undergo a phase transition from a non-ferroic to a ferroic state with change in the temperature or pressure. For ferromagnetic and ferroelectric materials, this phase transition occurs at a well-defined temperature known as the Curie temperature. In the following discussion, concepts of the ferroelectrics and ferro (ferri) magnetic materials will be discussed in detail.

1.3. Ferroelectric and Antiferroelectric Materials

A material, showing spontaneous polarization which can be reversed with the application of an external electric field is known as ferroelectric material. The ferroelectric phenomenon is usually observed in polar class of non-centrosymmetric crystal [Jaffe et al. (1971)]. Ferroelectrics are defined by a hysteresis curve between electric field (E) and polarization (P) develops from the spontaneous polarization (P_s) in each unit cell of ferroelectric material. The electric dipoles in the domains begin to orientate when electric field is applied on these materials. The value of net polarization decreases, with the reversal of the electric field. Some polarization remain present even after applied field return to zero, known as remnant polarization P_r. The net polarization reduces to zero by applied electric (negative field), which is known as coercive field E_C. The mechanism is displayed in the fig. 1.1.

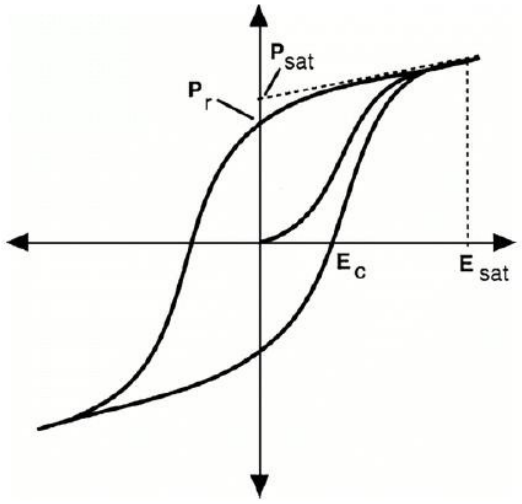

Fig.1.1 Hysteresis loop for ferroelectric material (Polla, 1998)

The other intrinsic property is temperature dependence of the dielectric constant (ε_r) above the Curie temperature i.e. in paraelectric region governed by the Curie-Weiss law.

A ferroelectric material go through a phase transition from a paraelectric phase to ferroelectric phase by the evolution of a polar axis via a structural phase transition at a characteristic temperature called 'Curie point' (T_0). Above Curie point, hysteresis loop disappears. The phase transition from paraelectric to ferroelectric is accompanied with a pronounced dielectric anomaly. Above the transition temperature, the dielectric constant obeys Curie-Weiss law, i.e.

$$\varepsilon_r = \frac{C}{T - T_C} \qquad (1.1)$$

where ε_r is dielectric constant of material, C is the Curie constant and T_C is the Curie-Weiss temperature. For second order ferroelectric transitions; in which properties such as lattice constant, polarization etc. change continuously with temperature; the two

temperatures are identical i.e. T_C=T_0. Whereas, in the first order ferroelectric phase transition (in which lattice constant, polarization etc. changes discontinuously), the Curie point and Curie temperature are not same but the Curie temperature (T_C) is always lower than Curie point (T_0) [Lines et al. (1977)].

1.4 Ferromagnetic and antiferromagnetic materials

Ferromagnetism is defined as the presence of spontaneous magnetization in absence of an external magnetic field whose orientation can be switched by the applied magnetic field followed by a hysteresis. As proposed by Weiss, origin of this spontaneous magnetization can be explained due to an internal 'equivalent molecular field' which tends to align the magnetic moments parallel to each other [Cullity (1972)]. The origin of the molecular field has been found to be quantum mechanical exchange energy, which causes spin of the electrons to align parallel or anti parallel. With the increase in the temperature, degree of alignment of the atomic magnetic moments decreases i.e. it becomes disordered and the ferromagnetic state transform to a paramagnetic state at higher temperatures. The temperature at which this transition takes place is known as the Curie temperature (T_C). Above T_C the susceptibility varies according to the Curie- Weiss law given by

$$\chi = \frac{C}{T - T_C} \qquad (1.2)$$

As-synthesized samples of ferromagnetic materials often show absence of a macroscopic magnetization because domains of magnetization are oriented in different directions. The following alignment and reorientation of the domains, results in a hysteresis in the magnetization (M) vs applied magnetic field (H) as shown in Fig. 1.2.

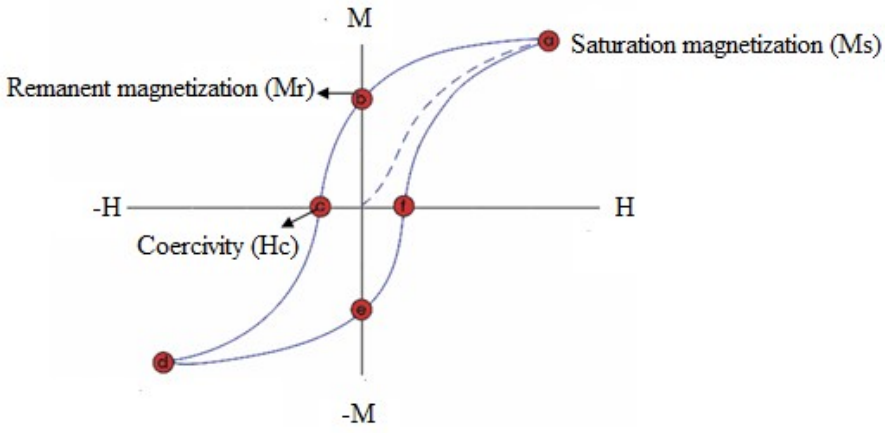

Fig.1.2 M-H hysteresis loop of a ferromagnetic material.

When the alignment of the spin moments of neighbouring atoms is antiparallel to each other, it is termed as antiferromagnetism**.** No net magnetic moment is associated in this case. There are several methods of organizing an equal number of down and up spins depending on the types of crystal lattice system in which the spins are to be arranged. These types of ordering result in different types of antiferromagnetic arrangement (A, C, G or E-type) as shown in Fig. 1.3. Antiferromagnetic order vanishes above a critical temperature known as the Néel temperature. Above the Néel temperature (T_N), the material behaves like a typical paramagnet. A plot of inverse of susceptibility (χ^{-1}) versus temperature (T) is a straight line in antiferromagnets, above T_N this line extrapolates to negative Curie temperature ($-T_C$) at $1/\chi = 0$. Above T_N, it obeys the Curie-Weiss law.

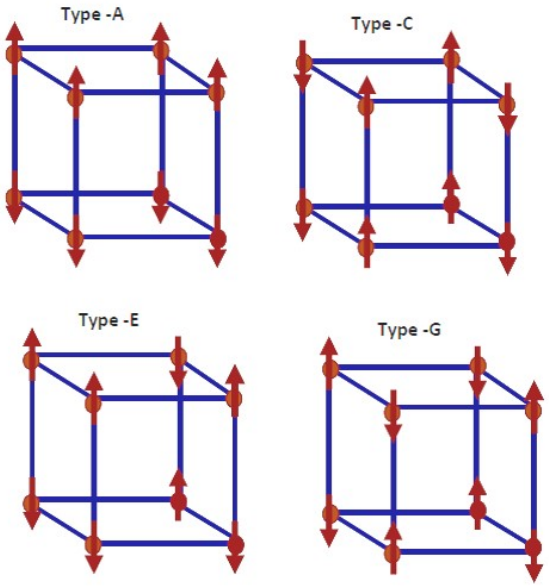

Fig. 1.3 Different type of antiferromagnetic ordering [drawn using convention of Wollen et al. (1955)].

Although, one does not expect net magnetization in the antiferromagnetic materials, it may exhibit net magnetization due to spin canting, lattice defects and frustrated surface spins in the absence of applied magnetic field. At sufficiently high magnetic fields, the spin direction of one of the magnetic sublattices may rotate and eventually lead to the 'spin flop' where all the spins would be aligned in a parallel fashion. Because of this rotation and spin flop, magnetization may be influence by an extrinsic magnetic field. The temperature dependence of the magnetization (M) and χ^{-1} for ferromagnetic and anti ferromagnetic materials are shown in Fig. 1.4 (a) and (b) respectively.

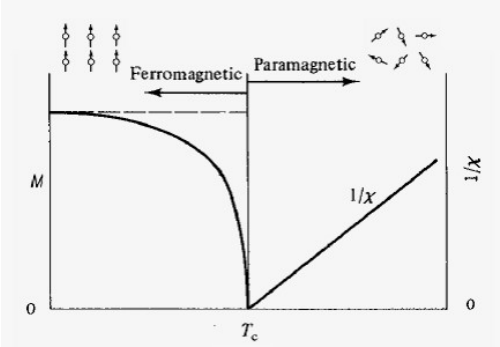

(a)

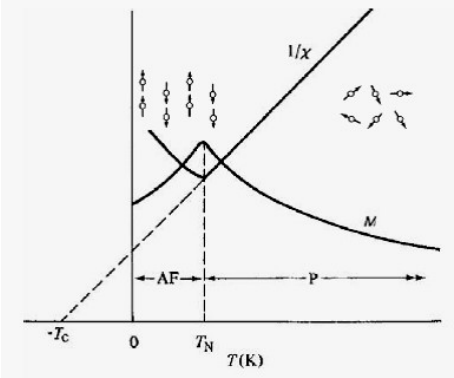

(b)

Fig.1.4 Temperature dependence of magnetization (M) and the inverse of the magnetic susceptibility (χ^{-1}) for (a) ferromagnetic and (b) antiferromagnetic material (schematic). AF = antiferromagnetic and P = paramagnetic [after Cullity (1972)].

1.5 Magnetic exchange interactions

Exchange interactions are accountable for long range ordering of magnetic moments. The coupling of magnetic moments is known as exchange interaction, essentially an outcome of overlap of electronic orbitals and given by exchange integral. We list below the different types of exchange interactions which lead to long range magnetic order state.

1.5.1. Direct exchange interaction

When the electrons on adjacent magnetic ions are close enough to have sufficient overlap of their wave functions they interact via exchange interaction. Such an interaction is

known as direct exchange. It allows a strong short range coupling, which reduces quickly on increasing the separation between the magnetic ions. For direct exchange interaction, the exchange integral J_{ex} can be negative or positive depending upon the stability between Coulombic and kinetic energies (K.E.). In the frame work of Ising model

$$E_{ex} = - J_{ex} S_i . S_j \qquad (1.3)$$

Where E_{ex} is the exchange energy, S_i and S_j are the electronic spins at the atomic sites which can take values +1/2 or -1/2. [Cullity (1972)]

1.5.2 Indirect exchange interaction

The indirect interaction amongst magnetic ions can be arbitrated through the conduction electrons as well in some cases. The spin-polarizes the conduction electrons through localized magnetic moment and this polarization couples to the adjacent confine magnetic moment at 'r' distance. Thus the exchange interaction is an indirect one and it not associated with direct coupling between the magnetic moments. This type of interaction is commonly known as Ruderman-Kittel-Kasua-Yoshida (RKKY) interaction (or also as itinerant exchange interaction) [Ruderman et al. (1954); Kasuya (1956); Yosida et al. (1957)], named after the discoverers of the effect. The RKKY type exchange coupling $J_{RKKY}(r)$ is given by [Blundel (2001)].

$$J_{RKKY}(r) \alpha \, Cos\,(2k_F r)/r^3 \qquad (1.4)$$

Where r (assuming spherical Fermi surface of radius k_F). The RKKY correlation, shown in Fig.1.5, is a long ranged and has damped oscillatory dependence on the separation between the magnetic moments. So, depending on the separation between a pair of magnetic ions, coupling between them can be of ferromagnetic or antiferromagnetic in nature.

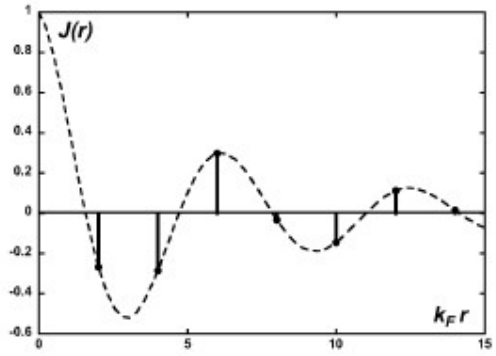

Fig.1.5 The coefficient of RKKY versus the inter-atomic distance r [after Honer (2005)]

1.5.3 Superexchange interaction

Superexchange describes the interaction between moments of ions which are too far apart to be influence by direct exchange, but couple over a relatively long distance through a non-magnetic ion which is situated in between the magnetic ions [Anderson (1950)]. For example, MnO and MnF_2 are both antiferromagnets, in view of that no direct overlap between the electrons on Mn^{2+} ions in each system. If the system is ideally ionic, then single unpaired electron in a d orbital will be present in each metal ion whereas oxygen shows two p electrons occupied in outer most states. The strength of the anti-parallel coupling between metal ions (M) depends on the bond length and bond angle M-O-M and is generally maximum when this bond angle is 180^0 i.e. the spins are collinear.

1.5.4 Double exchange interaction

In few oxides, the ferromagnetic exchange interaction is possible due to the occurrence of magnetic ions showing mixed valence i.e., it can present in oxidation state of more than one. For example, the ion of Mn can exist in oxidation states as Mn^{3+} or Mn^{4+}, in the mixed manganite system $La_{1-x}Sr_xMnO_3$. The ferromagnetic alignment in such systems is because of double exchange mechanism [Zener (1951)]. This can be understood with help of Fig.1.6. In the case of mixed valence of Mn ion, eg electron on Mn^{3+} ion can hop to a

neighbouring site Mn^{4+} via oxygen by interacting with 2p electrons of O^{2-}. This is possible only if there is a vacancy of the same spin. However, because of the strong Hund's coupling, the three electrons in the t_{2g} level want to keep the e_g electron aligned to them. Hence it is not suitable for an electron (e_g) to hop to an adjacent ion in which it is antiparallel to the t_{2g} spins. The ferromagnetic alignment of adjacent ions is needed to continue the high-spin arrangement on both the receiving and donating ions. This model is superficially similar to superexchange. In superexchange, an antiferromagnetic (in general) or ferromagnetic alignment occurs between two atoms with the same valence, while in double exchange, the interaction occurs only when one atom has an extra electron compared to the other.

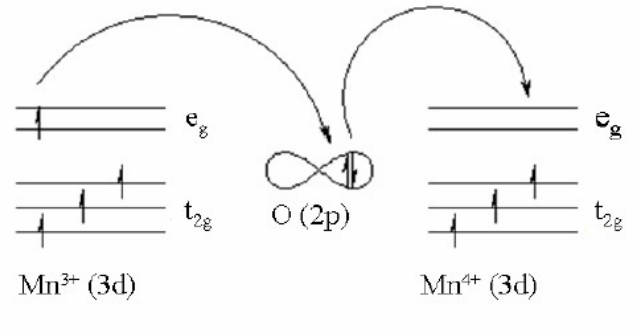

Fig. 1.6 Double exchange interaction [after Zener et al. (1951)].

1.5.5 Anisotropic exchange interaction

In an antiferromagnetic system the appearance of weak spontaneous magnetization arises due to the magnetic moments which are not collinear, i.e. canted with respect to each other. This type of canted antiferromagnetic are called as weak ferromagnets. Two inputs are compulsory for canting of spin: (i) the existence of two nonsymmetry associated nearest-neighbour magnetic ions and (ii) antisymmetric exchange and/or single ion anisotropy. Antisymmetric exchange depends upon symmetry arguments defined by Dzyaloshinskii (1958), while Moriya (1960) explained the phenomenon as individual spins interacting through spin-orbit coupling. The fusion of these arguments shows the anisotropic exchange interaction, which is commonly known as the Dzyaloshinskii-Moriya (DM) interaction. For describing the symmetric exchange (spin-spin interaction) the general Hamiltonian used is $H = -J\Sigma S_i.S_j$, which does not allow the canting of the spins and produce natural parallel or anitiparallel alignments of spins. The D-M interaction, on the other hand, is expressed by an additional term in the Hamiltonian given as [Moriya (1960)]

$$H_{D\text{-}M} = D_{ij}.\ |S_i \times S_j| \qquad (1.6)$$

Where D_{ij} is a DM constant vector. Due to interplay between superexchange and spin-orbit coupling the DM interaction arises. This interaction begins the spin to cant thus reducing the coupling energy between S_i and S_j. Since the magnitude of D_{ij} is proportional to (g-2)/g, where g is Lande g-factor, it is noticeable when g changes significantly from 2. When the superexchange interaction is mediated through oxygen, it is also proportional to the position of oxygen between the two magnetic ions i.e. $D_{ij}\ \alpha\ x \times r_{12}$ where r_{12} is the vector line connecting along the two magnetic ions and x is the displacement of oxygen from this line (see Fig. 1.7).

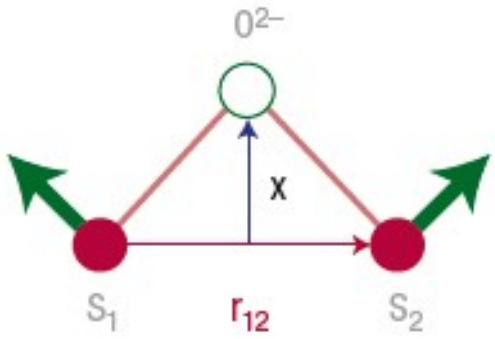

Fig.1.7 Effect of asymmetric Dzyaloshinskii-Moriya (D-M) interaction [after Cheong et al. (2007)].

1.6 Multiferroic Materials

Multiferroic materials may be defined as single phase materials, in which two or all three of primary ferroic properties such as: ferroelectricity, ferromagnetism, and ferroelasticity occur in the same phase. However, in recent years, anti-ferromagnetism, anti ferroelectricity, ferrimagnetism and ferrielectricity has also been included in the definition of multiferroics [Eerenstein (2006)]. In the multiferroics, if there exists a coupling between at least two ferroic properties e.g. a coupling between ferroelectric and magnetic order parameters such that the magnetic polarization can be switched by the application of an electric field and ferroelectric polarization by the application of a magnetic field are known as magnetoelectrics.

1.7 Magnetoelectric coupling in multiferroic materials

The coupling between two ferroic orders such as polarization (P) and magnetization (M) in a material is generally termed as magnetoelectric effect i.e. the application of electric field (E) can induce magnetization (M) and the application of magnetic field (H) can

induce polarization (P). According to Landau theory, the free energy of a magnetoelectric multiferroic can be expressed as following [Fiebig (2005); Wang et al. (2009)] i.e.

$$F(E,H) = F_0 - P_i^s - M_i^s H_i - \frac{1}{2}\varepsilon_0 \varepsilon_{ij} E_i E_j - \frac{1}{2}\mu_0 \mu_{ij} H_i H_j - \alpha_{ij} E_i H_j$$
$$\frac{1}{2}\beta_{ijk} E_i H_j H_k - \frac{1}{2}\gamma_{ijk} H_i E_j E_k - \quad (1.7)$$

Where, F_0 denotes the ground state free energy of the system and the components of electric (E) and magnetic (M) fields are denoted by (E_i, E_j, E_k and H_i, H_j, H_k) respectively. The corresponding components of spontaneous magnetization (M^s) and polarization (P^s) and are denoted by M_i^s and P_i^s. The entities ε_{ij} and μ_{ij} are second rank tensor and stand for the electric and magnetic susceptibility of material while ε_0 and μ_0 are the susceptibilities of vacuum. The coefficient α_{ij} is again a second rank tensor that defines the linear magnetoelectric effect and the coefficients β_{ijk} and γ_{ijk}, a third rank tensor, define the quadratic magnetoelectric coupling. By differentiating equation (1.7) partially w.r.t. E_i or H_i and setting E_i or H_i =0, we can obtain the magnetoelectric effects in terms of $P_i(H_i)$ or $M_i(E_i)$.

The ability to couple the magnetic and the electric polarization in magnetoelectric multiferroics offers an extra degree of freedom in the design of actuators, transducers, and storage devices. Specific device applications that have been suggested for such magnetoelectric multiferroics include multiple state memory elements (corresponding to +P, -P, +M and –M states), electric-field controlled ferromagnetic resonance devices, transducers with magnetically modulated piezoelectricity [Fiebig (2005); Ramesh and Spaldin (2007); Wang et al. (2009);] etc.

1.8 Incompatibility between magnetism and ferroelectricity

The coexisting ferroelectricity and magnetism in a single phase magnetoelectric multiferroic material offers great challenges to the condense matter physicists. It has been proved that in ABO_3 perovskites system ferroelectricity is driven by the off-centering displacement of B-site transition metal (TM) ions that requires vacant d-orbitals (d^0) so that it (TM) could established covalent bonding with neighboring oxygen atoms via the hybridization of $3d^0$ orbital of Ti and 2p orbitals of oxygen in case of $BaTiO_3$ and $PbTiO_3$ [Cohen (1992)]. In addition to this, the evolution of ferroelectric state breaks the spatial inversion symmetry also. On the other hand, evolution of magnetic ordering requires transition metal cations having partially occupied d-orbitals (d^n electrons) along with the broken time reversal symmetry. These two phenomena, which seem to be mutually forbidden in a single phase material, have been shown to coexist in few magnetoelectric multiferroics that should violate both the symmetries of space and time i.e. spatial inversion and time reversal. This implies that in magnetoelectric materials in which the ferroelectric distortion is not caused by the hybridization of transition-metal ions in a noble gas configuration.

1.9 Approaches to the co-existence of the magnetism and ferroelectricity

As we have discussed in the preceding section, the vacant d-orbital of the B-site transition metal ions are the requirement to stabilize the ferroelectric state in ABO_3 Perovskites. Such kind of B-site cation excludes the magnetism in material. While this argument suggests that ferroelectric and magnetic ordering are absolutely incompatible, new mechanisms of ferroelectricity different from the conventional one have been identified in recent years which make the two otherwise mutually exclusive phenomena to occur in the same material.

1.10 Paramagnetic doping

Initial step towards the study of multiferroics perovskite was preceded by Russian scientists [Venevstev (1960)]. They suggest to combine the B-site of ABO_3 perovskite with transition metal cations having both the partially filled (d^n) and empty (d^0) d orbitals, where d^n and d^0 electronic configuration of the transition metal cations drive the ferromagnetism and ferroelectricity respectively. It was hoped that a coexistence of 'conventional' ferroelectricity and magnetism is possible (i.e. Partial substitution of ferroelectrically active transition metal ions (d^0) by magnetically active transition metal ions (d^n electronic configuration) with maintaining the stability of perovskite structure). This idea has worked and multiferroicity has been reported in site-disordered compounds like $Pb(Fe_{0.5}Nb_{0.5})O_3$ (PFN) and $Pb(Fe_{2/3}Nb_{1/3})O_3$ (PFW) in which ferroelectricity is driven by Nb^{5+} and W^{+6} ions while magnetism is driven by Fe^{3+} ions [Fiebig (2005); Wang et al. (2009); Singh et al.(2010)]. However, the magnetic transition temperature in these materials occurs well below the room temperature.

1.11 Multiferroic materials with improper ferroelectricity

In the previous section, it has been discussed that the electric polarization is the primary order parameter that drive the ferroelectric transition. These ferroelectrics are termed as 'proper' ferroelectrics. There are some other types of the ferroelectrics in which polarization is induced by some secondary effect (not the polarization as primary order parameter) such as lattice distortions, charge ordering and some kind of magnetic ordering etc. This group of materials was termed as 'improper' ferroelectrics. Some example of the proper and improper ferroelectricity is given in the Table 1.1 [After Cheong and Mostovoy (2007)].

Table 1.1. Classification of ferroelectrics [after Cheong et al. (2007)]

Classification of ferroelectrics		
Mechanism of inversion symmetry breaking		Materials
Proper	Covalent bonding between $3d^0$ transition metal (Ti) and oxygen	$BaTiO_3$
	Polarization of $6S^2$ lone pair of Bi or Pb	$BiMnO_3$, $BiFeO_3$, $Pb(Fe_{2/3}W_{1/3})O_3$
Improper	Structural transition 'Geometric ferroelectrics'	K_2SeO_4, $CsCdl_4$ Hexagonal $RMnO_3$
	Charge ordering 'Electronic ferroelectrics'	$LuFe_2O_4$
	Magnetic ordering 'Magnetic ferroelectrics'	Orthorhombic $RMnO_3$, RMn_2O_5, $CoCr_2O_4$

1.12 Ferroelectricity induced by lone-pair electrons

The mechanism of ferroelectricity is based on cations that have an $(ns)^2$ (lone pair) valence electron configuration. Such lone-pair is generally unstable and hence to get a stable state it mixed itself with a low-lying $(ns)^1(np)^1$ excited state that breaks the spatial inversion symmetry also [Atanasov (2001)]. This 'stereochemical activity of the lone pair' is the driving force for the off-centre distortion and, in turn, the ferroelectricity [Hill (2000)]. Examples of such kind of systems are $BiFeO_3$ and probably $BiMnO_3$, where magnetism and ferroelectricity are caused by B-site cations and stereochemically active lone pair of A-site cation, respectively [Wang et al. (2003); Hill (2000)]. In this class of materials, $BiFeO_3$ is unique as it shows the multiferroicity at room temperature because of its shows high temperature magnetic transition at 643K [Roginskaya et al. (1966)] and ferroelectric transition at 1103K [Kaczmarek et al. (1975)].

1.13 $BiFeO_3$ as a multiferroic material

As mentioned earlier, magnetoelectric multiferroics $BiFeO_3$ has received tremendous attention out of all multiferroic materials, as a multiferroic material available at room temperature. It shows ferroelectric transition (T_C) ~1103 K [Kaczmarek et al. (1975)] and antiferromagnetic ordering (T_N) at ~643 K [Roginskaya et al. (1966)] well above the room temperature. This increases the possibility of developing new kinds of potential devices based on magnetoelectric coupling.

$BiFeO_3$ shows rhombohedrally distorted perovskite crystal structure which belongs to R3c space group [Jacobson et al. (1975); Fischer et al. (1980); Kubel (1990); Sosnowska et al. (2002)]. The hexagonal lattice parameter are a_{hex} =b_{hex}=5.58102(4), c_{hex} =13.8757(4), α=β=90° and γ=120° [Palewicz et al. (2007)]. The hexagonal unit cell contains six formula units whereas unit cell of rhombohedral, contains two formula units appearing from counter-rotations of neighboring oxygen octahedra about the trigonal $[111]_{pc}$ axis as shown in Fig. 1.8. The spontaneous polarization developed along $[111]_{pc}$ in R3c symmetry and Bi, Fe, and O are displaced relative to one another along this threefold axis [Palewicz et al. (2007)].

The ferroelectric characterization of $BiFeO_3$ has show a very difficult task from experimental point of view, because of high conductivity of $BiFeO_3$. In spite of large ionic displacements in the ferroelectric phase and high ferroelectric Curie temperature, the measurement on bulk single crystal shows a very small polarization. Teague el al. (1970) initially reported the value of spontaneous polarization i.e. 6.1 $\mu C/cm^2$ which was measured along the $[111]_{pc}$ direction in the single crystal of $BiFeO_3$ at liquid nitrogen temperature.

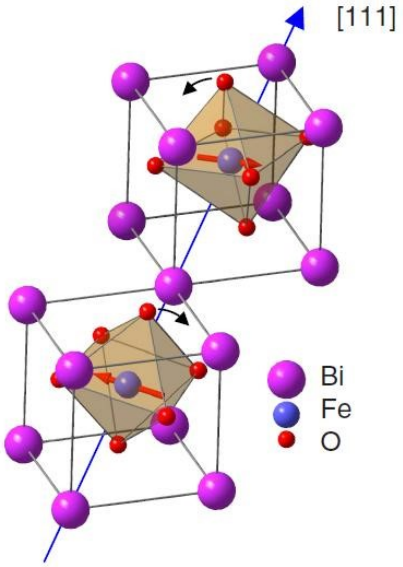

Fig.1.8 Crystal structure of bulk $BiFeO_3$ at room temperature. Two simple perovskite unit cell are shown to illustrate that the successive oxygen octahedral along the polar [111] axis rotate with opposite sense. Arrows on Fe atoms indicate the orientation of the magnetic moments in the (111) plane [after Lubk et al. (2009)].

This value is significantly less than the expected value based on the structural data. Wang et al. (2003) have reported a very high value of P_S ~55 μC/cm^2 (see Fig. 1.9) and 150 μC/cm^2 [Yun et al. (2004)] for the thin film of $BiFeO_3$. This enhancement of polarization value for thin film over bulk sample of $BiFeO_3$ is due to the structural change as the symmetry of thin film of $BiFeO_3$ was found to become pseudo-tetragonal (strictly speaking monoclinic) due to the introduction of strain by the substrate or electrode. Initially first-principles calculations have shown that the spontaneous polarization of even the rhombohedral structure of $BiFeO_3$ can reach 90–100 μC/cm^2 [Neaton et al. (2005); Ravindran et al. (2006)].

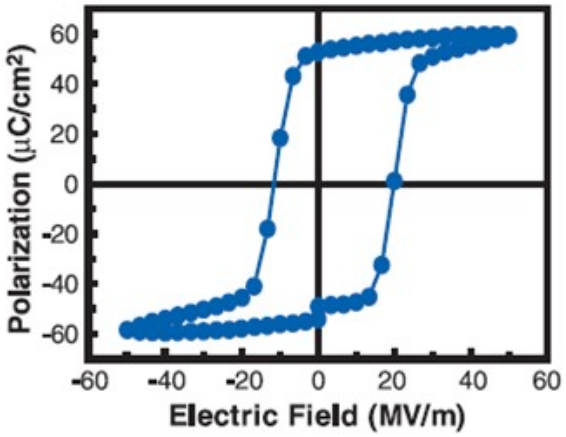

Fig.1.9. Ferroelectric hysteresis loop measured at 15 kHz for thin film grown on (100) oriented substrat $SrTiO_3$ [after Wang et al. (2003)].

The polarization values as high as 100 μC/cm^2 has been reported [Lebeugle et al. (2007)] along the direction of $[111]_{pc}$ on single crystal of $BiFeO_3$. The crystals were prepared from the flux of Bi_2O_3-Fe_2O_3 having a growth temperature of 1123 K. This work shows $BiFeO_3$ have high polarization, suggesting it to be an intrinsic property of it rather the effect of strain as reported for $BiFeO_3$ thin films.

Apart from ferroelectric behaviour, $BiFeO_3$ is also well known to reveal an antiferromagnetic ordering. Sosnowska et al. (1982) studied the magnetic structure of $BiFeO_3$ and showed that the Fe magnetic moments are coupled ferromagnetically within the pseudocubic $[111]_{pc}$ planes and antiferromagnetically between adjacent planes, as shown in Fig 1.10.

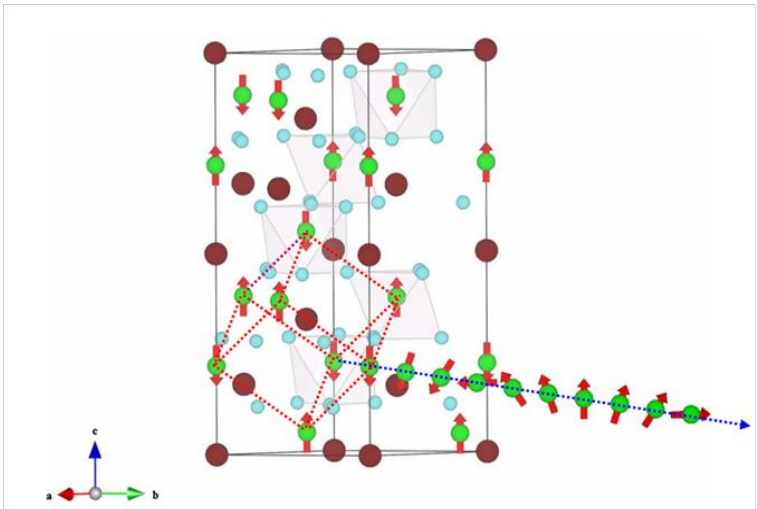

Fig.1.10 $BiFeO_3$ lattice with bismuth (large circles), iron (large circles with arrow) and oxygen ions (small circles) are shown in hexagonal settings [after Park et al. (2011)]. The arrow at the Fe sites indicates the magnetic moments. The magnetic cell (dashed lines) is shown for a G-type antiferromagnetic structure. The propagation wave vector of the incommensurate spiral spin structure k is along the [110]h direction and lies in the plane of spin rotation (1-10)h.

This magnetic order corresponds to G-type antiferromagnetic structure with respect to the elementary perovoskite cell. If the magnetic moments are oriented perpendicular to the $[111]_{pc}$ direction (i.e. in the $(111)_{pc}$ plane, the symmetry also permits canting of the magnetic moments due to Dzyaloshinski-Moriya interaction resulting a weak ferromagnetism. However, it was also found that superimposed on the antiferromagnetic ordering, there is a spatially modulated spiral spin structure in which the antiferromagnetic axis rotates through the crystal with an incommensurate long-wavelength period of ~620 Å [Sosnowaska et al. (1982)]. The propagation wave vector k lies in the plane of spin rotation $(1\text{-}10)_h$ and along the $[110]_h$ direction as shown in Fig. 1.11.

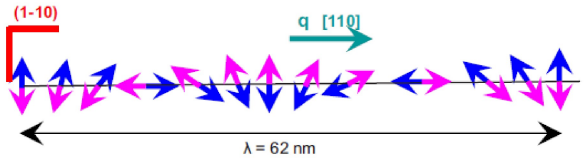

Fig. 1.11 The propagation vector is along the direction [110] and the plane of spin-rotation is (1-10) [Lebeugle et al. (2007)].

The presence of the modulated magnetic ordering has also confirmed by NMR [Zalessky et al. (2000); Kozheev et al. (2003)] and EPR [Ruette et al. (2004)] studies in $BiFeO_3$. The spiral modulated spin structure leads to cancellation of any macroscopic magnetization due to this canting. Due to the existence of spiral spin structure, the field dependent magnetization values revealed a pure antiferromagnetic response [Lebeugle et al. (2007)] as shown in Fig. 1.12, in the absence of any sign of weak ferromagnetism in single crystal pure $BiFeO_3$. Weak ferromagnetism reported in pure $BiFeO_3$ samples in polycrystalline form [Zhang et al. (2005)] is mostly due to the presence of some magnetic impurity.

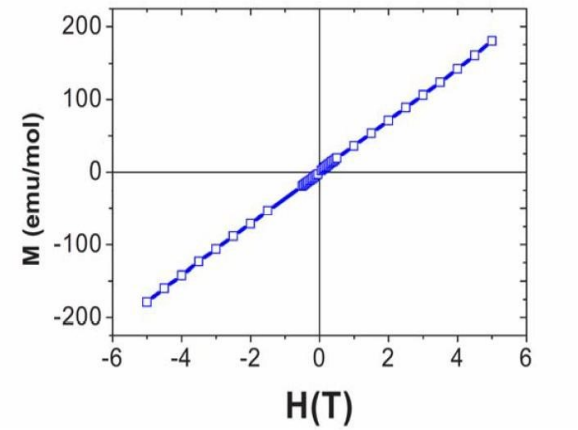

Fig.1.12 Magnetization versus applied magnetic field curve of the powder sample measured at 300K [after Lebeugle et al. (2007)].

1.14 High temperature study of $BiFeO_3$

There are still many contradictions about the high-temperature phases of bulk $BiFeO_3$. [Palai et al. (2008)] have carried out complete study of the phase diagram of $BiFeO_3$ based on spectroscopic, thermal analysis, diffraction and other methods. There are three distinct solid phases above room temperature and below the melting point (~960℃): the rhombohedral α-phase, below T_C, an intermediate β phase, in the region 830 ℃-925℃, and a cubic γ-phase in the region 925℃-933℃ before decomposition and subsequent melting. Based on polarized light and Raman measurements they suggested that the symmetries of β and γ phases are orthorhombic and cubic, respectively [Palai et al. (2008)]. Whereas [Haumont et al.(2006)] proposed a cubic symmetry for β-phase. The tetragonal phase (space group I4/mcm) was predicted by using first principles calculations above T_C which is similar with antiferrodistortive motions, before transforming to a cubic phase at approximately 1167℃ [Kornev et al.(2007)]. Haumont et al. (2008) have proposed from a high temperature x-ray diffraction study, the monoclinic phase with pseudotetragonal character in the space group C2/m. Further, it was suggested that the true space group as P21/m. Selbach et al. (2008) found a first order phase change at T_C and they proposed that the paraelectric β-phase corresponds to the rhombohedral symmetry with centrosymmetric, space group R3c using high temperature x-ray diffraction study.

1.15 Magnetoelectric coupling in $BiFeO_3$

The presence of spatially modulated spiral spin structure inhibits linear magetoelectric (ME) coupling in $BiFeO_3$ but it can exhibit quadratic coupling coefficient [Schmid (1994)] which is quite weak. $BiFeO_3$ does not exhibit any macroscopic magnetization and linear magnetoelectric coupling due to presence of superimposed spiral spin structure.

The macroscopic magnetization and linear magnetoelectric coupling can be obtained by the suppression the magnetic spin spiral so that the latent magnetization due to canted spins is released. So in the literature, for the destruction of the spiral spin structure of pure $BiFeO_3$, five different ways have been proposed.

1.15.1 Making of thin film

The suppression of spiral spin structure may also possible under epitaxial constraints [Eerenstein et al. (2005)]. Saturation magnetization value of M_s ~$0.06\mu_B$/Fe has been reported in epitaxial films of $BiFeO_3$ [Eerenstein et al. (2005)]. The values of magnetization noticed for $BiFeO_3$ nanoparticles and epitaxial thin films are in good agreement with the theoretically calculated value of 0.1μB using first principles density functional theory [Ederer et al. (2005)]. Wang et al. also reported that saturation magnetization value of ~150 (emu)/cm^3 for 70 nm thick film of $BiFeO_3$, as film thickness increases to 400 nm, magnetization decreases to ~5 emu/cm^3 [Wang et al. (2003)]. The thin film of $BiFeO_3$ deposited on $(LaAlO_3)_{0.3}(Sr_2AlTaO_6)_{0.7}$ (001) substrate also shows suppressed spiral spin structure. The magnetic moment enhances with decreasing film thickness (fig. 1.13), i.e. for 65 nm it has been reported ~8 emu/cm^3 (~$0.06\mu_B$) that further increases to ~14 emu/cm^3 (~$0.1\mu_B$) for the 40 nm film [Rana et al.(2007)].

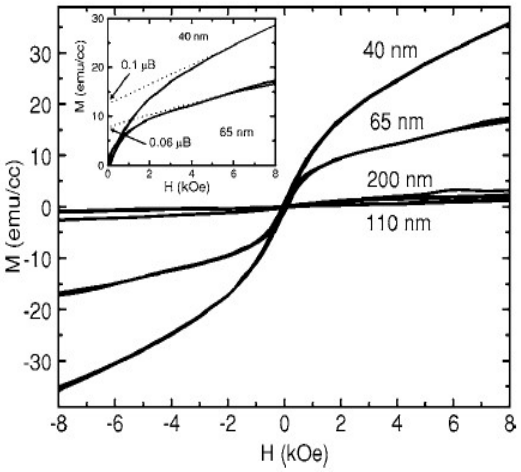

Fig.1.13 Magnetization vs magnetic-field at 300K for different size of $BiFeO_3$ thin films. The inset depicts that the linear part which arising from antiferromagnetic contribution[Rana et al.(2007)].

1.15.2 Application of high magnetic field

Above the certain critical field, the magnetoelectric coupling changes the sign through change in spin configuration. The field dependence of the longitudinal polarization in which magnetic field is applied along [001] axis is shown in Fig. 1.14(a). At $H < H_C$ the polarization is an essentially quadratic function of the field. However, on increasing the magnetic field above a critical value $H = H_C \sim 200$ kOe, the spatially modulated spiral spin structure is destroyed and leads to a remanent magnetization as shown in Fig. 1.18(b). Above this critical field $H_C \sim 200$ kOe, the electric polarization changes sign and becomes linearly dependent on magnetic field [Popov et al (1993)]. This experiment has conclusively established that linear magnetoelectric coupling in $BiFeO_3$ can be observed by the breaking the spatially modulated spin spiral structure leading to a homogeneous canted G-type antiferromagnetic structure. The linear magnetoelectric effect is absent in $BiFeO_3$, which has been established experimentally by several other workers as well [Tabares-Munoz et al. (1985); Kadomtseva et al. (2004)] for field below H_C.

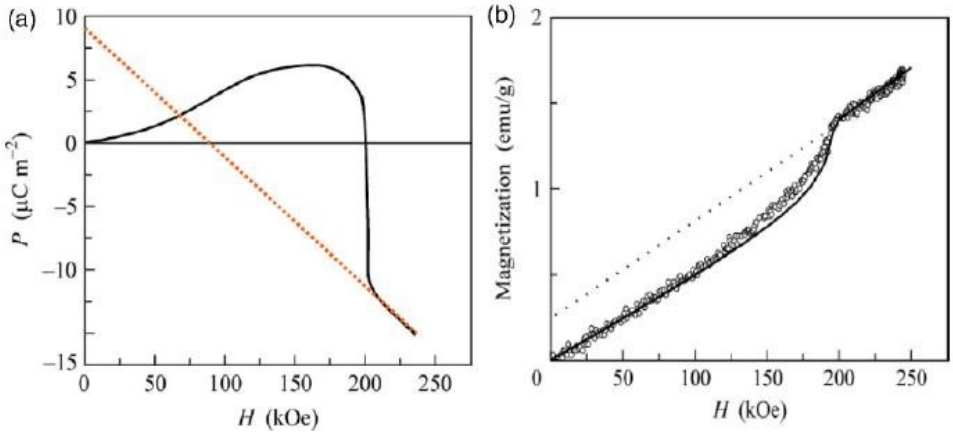

Fig.1.14 (a) Longitudinal polarization verses the strength of the magnetic field at 10 K [Popov et al. (1993)]. (b) Magnetization vs pulsed magnetic field for H ≤25T for a $BiFeO_3$ at 10 K [after Catalan et al. (2009)].

1.15.3 Doping in $BiFeO_3$

To get better results in ferroelectric and magnetic properties, Bi^{3+} and Fe^{3+} ion have been doped with rare- earth element, like Mn, La, Nb, Ba, Tb etc. Attempts have been made to synthesize pure phase of $BiFeO_3$ in order to suppress the spiral spin structure and improve the ferroelectric properties as well by increasing the resistivity. For example, La substituted $BiFeO_3$ ceramic powder was synthesized by solid-state reaction route shows that La substitution in $BiFeO_3$ increases both the ferroelectric and ferromagnetic properties. It has been reported that 20% La doped $BiFeO_3$ shows remnant magnetization of ~0.0736 emu/g, which is much better than pure $BiFeO_3$ powder [Das et al. (2007)]. In $La_xBi_{1-x}FeO_3$ powder with x = 0.4 shows maximum magnetic remanence (Mr), in the order of 0.274 emu/g at room temperature (see fig.1.15) [Suresh et al.(2013)]. In $Bi_{1-x}Ba_xFeO_3$ at x=0.25 exhibit magnetism and ferroelectricity simultaneously at room

temperature. $BiFeO_3$ with the rhombohedrally distorted structure allows a weak ferromagnetic ordering due to canting of the spins.

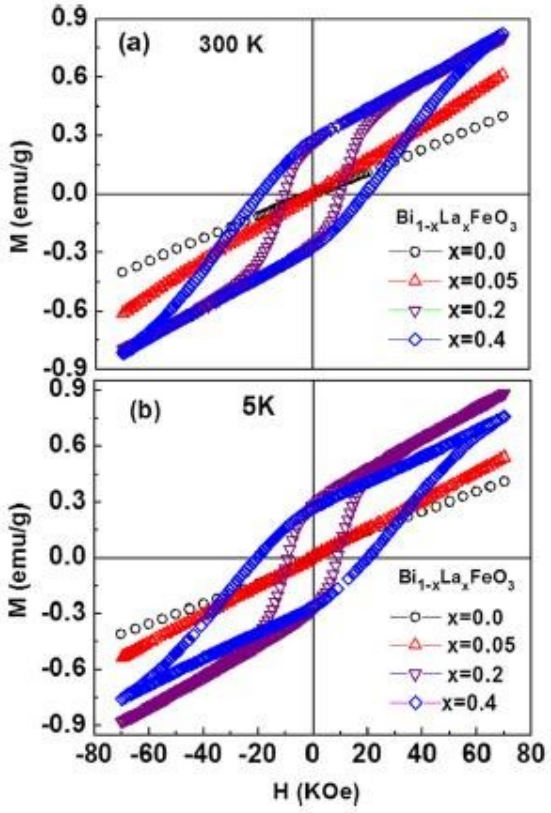

Fig. 1.15 M-H curves of $La_xBi_{1-x}FeO_3$ (x=0, 0.05, 0.2, and 0.4) at (a) 300K and at (b) 5K [after Suresh et al.(2013)].

With doping of Ba the structure of $BiFeO_3$ may be distorted, that caused bond angle of Fe–O–Fe to change, which can increase its magnetization [Wang et al.(2006)]. The 1% Nb-doped $BiFeO_3$ showed a ferromagnetic-like behavior with M_r=0.015 emu/g and H_c=500 Oe [Jun et al.(2005)]. The doping of Mn in Bi^{3+} sites in the $BiFeO_3$, can enhances both its saturation magnetization (from 0.53 to 2.54 emu/g) and remnant electric polarization (from 0.0811 to 0.6241 $\mu C/mm^2$) due to the magnetically driven distortion of spiral spin cycloid [Dhanalakshmi et al. (2016)]. In $BiFe_{0.90}Mn_{0.10}O_3$ thin film the

remnant magnetization value of was found to be approximately six times than that of pure $BiFeO_3$ thin film (i.e. ~154.04 emu/cm^3) under an applied magnetic field of 10 kOe. It may be due to the enhancement of super-exchange interaction between the Fe^{3+} (Mn^{2+}) and O^{2-} ions or may be structural distortion of spin cycloid [Zhang et al. (2018)].

1.15.4 Solid solutions of $BiFeO_3$ with other perovskite

The spiral spin structure suppressed with a non-zero remanent magnetization has been found in several other compounds, which modified $BiFeO_3$ solid solutions. The suppression of spiral spin structure in $BiFeO_3$-based solids was predicted theoretically by using first principles calculations on La doped $BiFeO_3$ [Lee et al. (2010)]. Apart from the enhancing magnetic properties, the solid solution of $BiFeO_3$ exhibits different structural transformations and some important interesting phenomenon with increasing concentration of the alloying component [Bhattachrjee et al. (2010); Rusakov et al. (2011)]. Formation of solid solutions of $BiFeO_3$ with several other perovskite oxides with superior dielectric properties has been reported using $PbZrO_3$ [Ivanov et al. (2008)], $Pb(Fe_{1/2}Nb_{1/2})O_3$ [Kiselev et al. (1969)], $Pb(Zr_xTi_{1-x})O_3$ [Korchagina et al. (2009)], PLZT [Kanai et al. (2001)], Choudhary et al. (2009)], $BaTiO_3$ [Kumar et al. (2000)], $PbTiO_3$ [Zhu et al. (2008); Bhattacharjee et al. (2010)], $BiCoO_3$ [Dieguez et al. (2011)], $NaNbO_3$ [Raevski et al. (2008)], $K_{0.5}Bi_{0.5})TiO_3$ [Bennett et al. (2013)] and $BiMnO_3$ [Pálová et al. (2010)]. Park et al. (2010) reported that the solid solution $BiFeO_3$ with hysteretic behavior having the values of $M_r \geq 0.32$ emu/g, which shows that the magnetization is released through destruction of spiral spin structure by introduction of even a very small amount of ferroelectric material $BaTiO_3$ (see fig. 1.16).

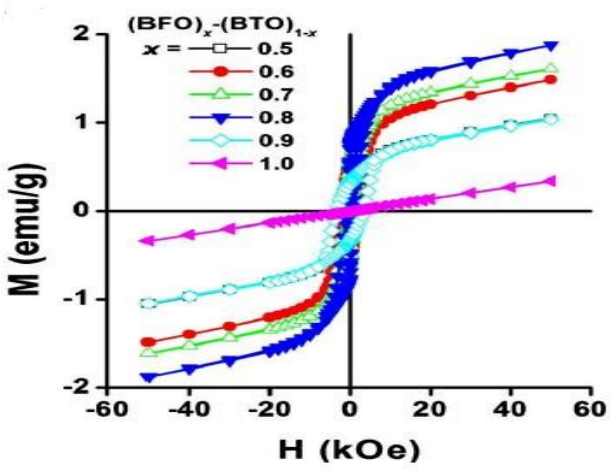

Fig. 1.16 Hysteresis loops for as prepared $(BiFeO_3)_x$-$(BaTiO_3)_{1-x}$ solid solutions with indicated x values at room temperature[Park et al. (2010)].

Singh et al. (2014) also observed that of the M-H curve with a small remanent magnetization in BF-xBT compositions with x≤0.50 suggests that the spiral spin structure of $BiFeO_3$ is melted away by the substitution of $BaTiO_3$. Form the fig.1.17, we can observe that, how the magnetization value change with increasing concentration of $BaTiO_3$.

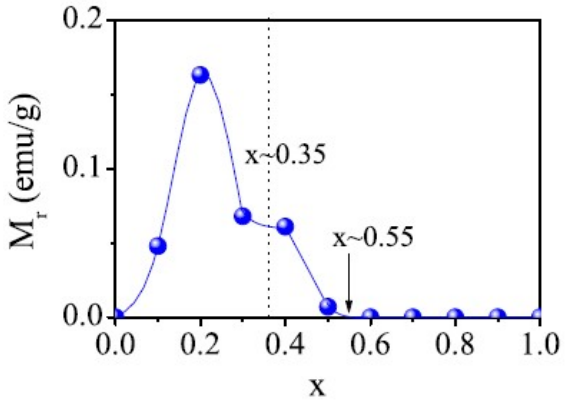

Fig. 1.17 Variation of remnant magnetization (Mr) of BF-xBT as a function of x at room temperature [Singh et al. (2014)].

1.15.5 Nano structured $BiFeO_3$

The spiral spin structure in $BiFeO_3$ can also be suppressed by reduction of particle size. The value of saturation magnetization (M_S) with size has been reported by different researchers [Park et al. (2007), Majumder et al. (2007), Goswami et al. (2011), Huang et al. (2013), Hasan et al.(2016)]. Park et al. have reported strong size-dependent magnetic properties [Park et al. (2007)]. They reported that with decreasing particle size, the suppression of the spiral spin structure increases and uncompensated spins and strain anisotropies are present at the surface. Fig. 1.18 shows that the magnetic response in $BiFeO_3$ can be developed when the particle size is less than 95 nm and it rapidly increases in the range of 270-460% for samples having particles size below 62 nm compared with that of the bulk powder. The value of saturation magnetization was 1.55 emu/g for14nm of $BiFeO_3$. Majumder et al. have obtained saturation magnetization value of ~ 0.40 μ_B /Fe for the size range of 4-40 nm of $BiFeO_3$ nano-particles, whereas in case of bulk it shows weak magnetization of the order of ~ 0.024 μ_B /Fe [Majumder et al. (2007)].

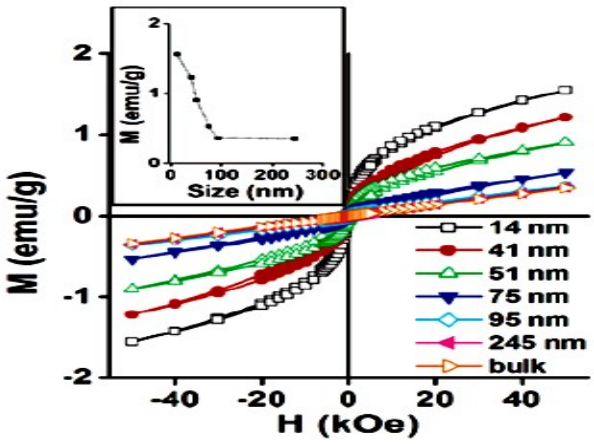

Fig. 1.18 Hysteresis loops at 300 K for $BiFeO_3$ nanoparticles with indicated sizes. The inset shows the magnetization behavior of as-prepared $BiFeO_3$ nanoparticles at 50 kOe as a function of size [Park et al. (2007)]

Hasan et al. also observe same kind of enhancement in saturation magnetization for the sol-gel synthesized $BiFeO_3$ powder. The magnetization value for 21 nm powders was 7.5emu/g and its value changes to 1.4 emu/g for 40 nm of $BiFeO_3$ [Hasan et al. (2016)]

1.16 Solid solutions of $BiFeO_3$ with $PbTiO_3$

Among the all ferroelectrics materials, $PbTiO_3$ is of particular interest owing to its high Curie temperature, large anisotropy and relatively low dielectric constant. $PbTiO_3$ undergoes structural phase transition at 490℃ from a high-temperature paraelectric phase to a low temperature ferroelectric phase [Remeika et al. (1970)]. It shows both large values of tetragonality (c/a=1.065) and spontaneous polarization ($P_s \approx 75 \mu C/cm^2$) along the c axis of tetragonal structure at room temperature [Gavrilyatchenko et al. (1970)]. The solid solution series of BF-xPT were first reported by Venevstev et al.(1960). It shows a Morphotropic Phase Boundary (MPB) [Fedelov et al. (1964), Smith et al. (1968), Zhu et al. (2008), Correas et al (2011)]. This solid solution become important due to co-existence of different ferroic orders and coupling between these ferroic orders. There is lots of research work carried out by different researcher on this system. Some of the works are discussed under following headings

(1) Stability of different structural phases as a function of composition

(2) Magnetic studies

(3) High temperature studies

1.16.1Stability of different structural phases as a function of composition

In general, an MPB can be defined as coexistence of two phases around a composition [Jaffe et al. (1971)]. The stability of tetragonal and pseudo-rhombohedral phases, which are present in BF-xPT solid solution are separated by MPB region [Fedelov et al. (1964), Smith et al. (1968), Woodward et al. (2003), Bhattacharjee et al. (2007), Zhu et al. (2008),

Correas et al. (2011), Kothai et al. (2013), (2014)]. The precise location of the MPB region has been a subject of intense investigation. Different researchers have reported different composition range of coexistence region in samples prepared by the conventional ceramic route. Fedelov et al. (1964) reported a composition range of coexistence of two phases which lie between 0. 27 < x < 0.34. He has given one of the early comprehensive results regarding the stability of both ferroelectric and magnetic phases against composition and temperature. According to this study a weak ferromagnetic phase coexist with the ferroelectric phase below room temperature in the composition range starting from x~0.27 to the $BiFeO_3$ end. Smith et al. (1968) have also carried out details studies on the structural properties of BF-xPT with composition and reported details of variation of unit cell parameters against composition at room temperature. In this study the two phase region is shown to consist of elementary tetragonal phase and unit cell doubled rhombohedral phase having qualitative similarity to the work by Fedelov et al. [Fedelov et al. (1964)]. The phase diagram presented by Smith et al is represented in fig. 1.19(a). Bhattacharjee et al. shown that in carefully prepared samples, the monoclinic and tetragonal phases are stable for x=0.27 and x=0.31, respectively and the width of MPB region is about 3% [Bhattacharjee et al. (2007)]. Zhu et al. reported that the MPB region extends to have unusually large width with $\Delta x=0.20$ in the BF-xPT system consists of tetragonal, rhombohedral and orthorhombic phases [Zhu et al. (2008)]. The phase diagram is shown in Fig.1.19 (b). The controversy related to width of MPB and the stability of different crystallographic phases still now not resolved. The reported works by Fedelov et al. (1964), Smith et al. (1968), Bhattacharjee et al. (2007) and Zhu et al. (2008) have used solid state reaction route to synthesize the various compositions for BF-xPT solid solution. On the other hand in a recent report,

compositions of BF-xPT, in entire composition range has been synthesized by mechanosysthesis method [Correas et al. (2011)] and they have reported a phase diagram qualitative similar to the early reports, but differs from that of Zhu et al. (2008). The phase diagram is shown in Fig. 1.19(c).

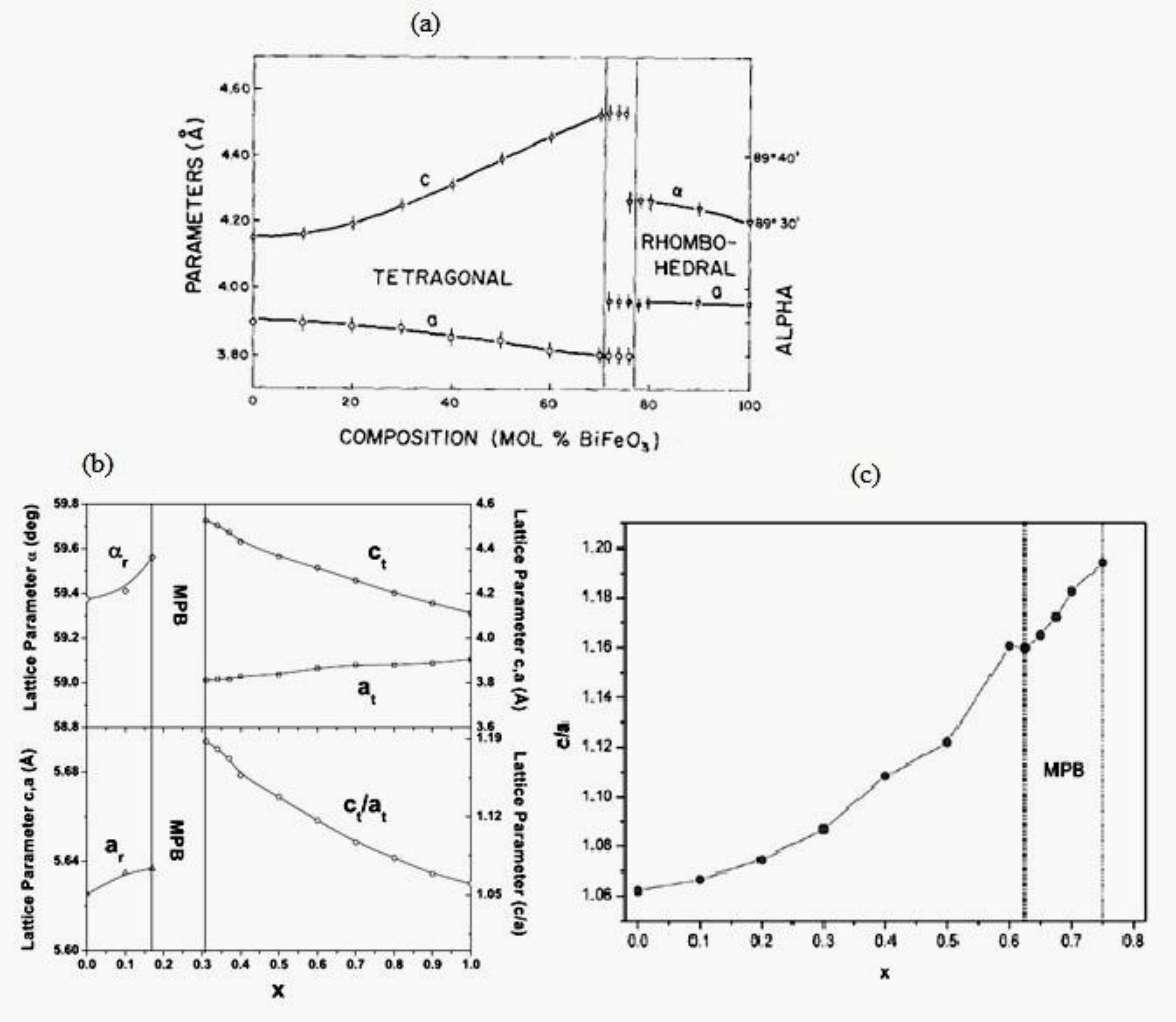

Fig.1.19 Variation of lattice parameters with composition in BF-xPT system as reported by different workers.(a) Smith et al. (1968) (b) Zhu et al. (2008) (c) Correas et al. (2011).

1.16.2 Magnetic studies

Zhu et al. used DC magnetization to study magnetic behavior of BF-xPT synthesized by solid state route. The first extensive magnetic phase diagram of this system was established by them and shown in Fig.1.20 [Zhu et al. (2008)] . The variation of magnetic moment with temperature shows three magnetic transitions and they have attributed these three transitions to the onset of long range antiferromagnetic ordering in three different phases in MPB region (see fig.1.21). Freitas et al. reported that the remnant magnetization increases with the decreasing of the $PbTiO_3$ concentration. The magnetizations were not saturated even after increasing magnetic field, indicating an antiferromagnetic nature. The observed remnant magnetizations ranging from 5×10^{-3} emu/g to 10×10^{-3} emu/g for all compositions [Freitas et al (2011)].

Bhattacharjee et al. have shown, with help of neutron diffraction study, that an abrupt change in magnetic structure from a collinear *G*-type antiferromagnetic to noncollinear antiferromagnetic one as the nuclear structure of the ferroelectric phase changes from tetragonal in P4mm space group to monoclinic in Cc space group across the MPB (see fig. 1.22). They have also reported an anomaly below the Neel transition (T_N) temperature which is termed as spin-reorientation phase transition (T_{OPT}) and it is due to spin flop of ferromagnetic component which are non-collinear (see fig. 1.23) [Bhattacharjee et al. (2010), Bhattacharjee et al.(2013)]. Golosovsky et al. have reported with help of neutron diffraction studies that the nanocrystalline powder of BF-xPT of size 20 to 50 nm exhibits both tetragonal and rhombohedra phases. A strong magnetic coupling between two parent phases observed due to size of crystalline [Golosovsky et al. (2015)]. Katoch et al. have reported two anomalies present during ZFC/FC measurements for single phase 0.80BF–0.20PT sample at 110 K and 220 K, whereas for 0.70BF–0.30PT sample which consist

two phase structure shows the anomaly at 255K (see fig.1.24). The magnetic anomalies of diffuse nature, indicates a local short range rearrangement of spins ordering within the antiferromagnetic state [Katoch et al (2016)].

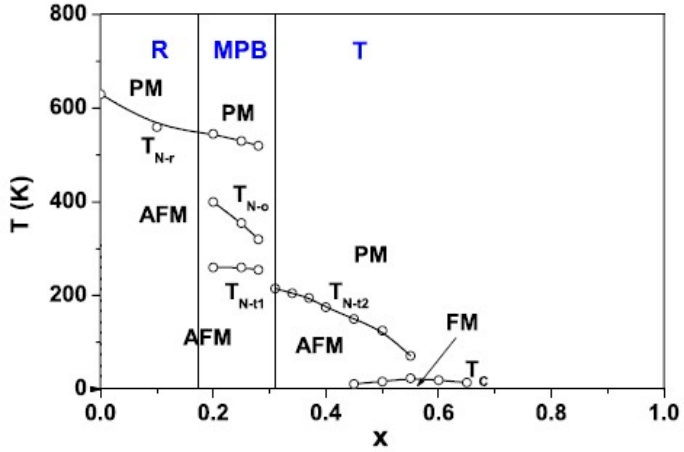

Fig. 1.20 Magnetic phase diagram of BF-xPT as reported by Zhu et al [after Zhu et al (2008)].

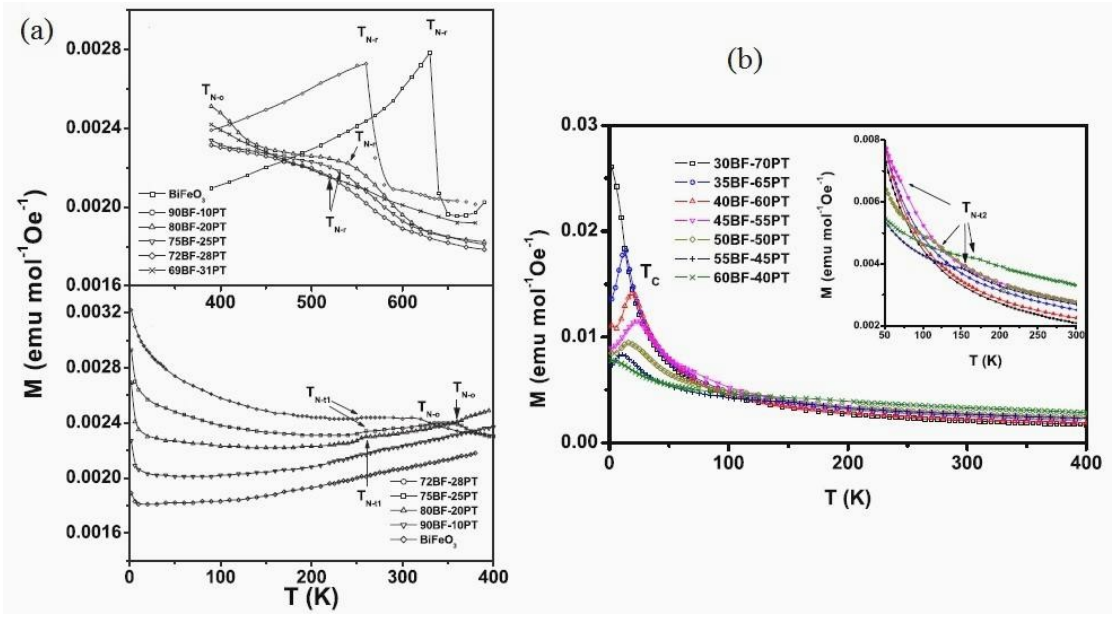

Fig.1.21 The variation of magnetization as a function of temperature for (a) rhombohedral (b) tetragonal phases of BF-xPT, as reported by Zhu et al. [Zhu et al (2008)]

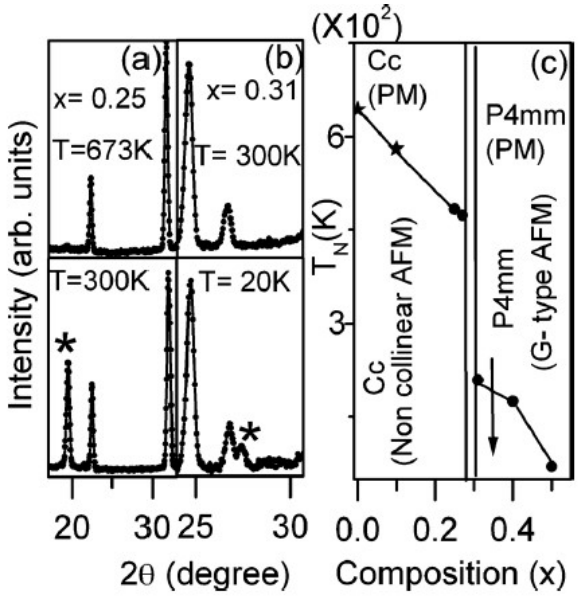

Fig.1.22 Powder neutron diffraction pattern of (a) BF-0.25PT and (b) BF- 0.31PT in the paramagnetic (upper panel) and magnetic (lower panel) phases. (c) The magnetic phase diagram of BF-xPT in the vicinity of the MPB [Bhattacharjee et al. (2010)].

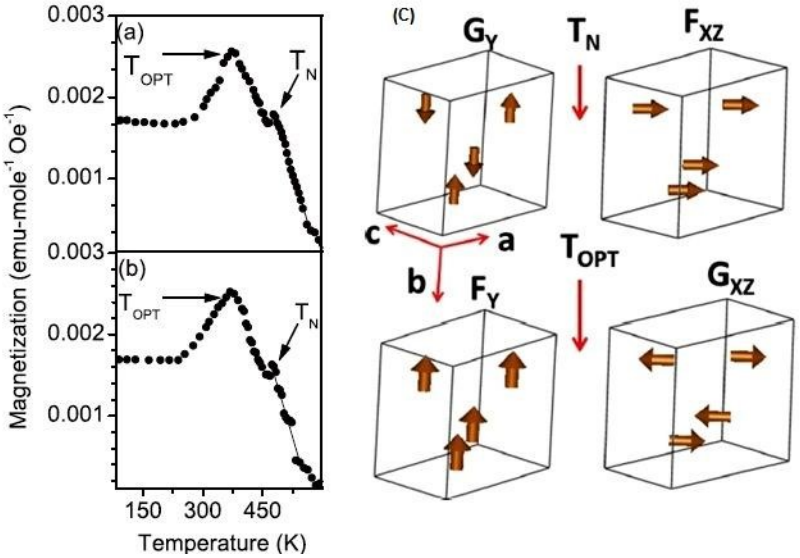

Fig.1.23 Temperature dependence of dc magnetization (M) of BF-xPT for (a) x = 0.25 and (b) x = 0.27 showing two transitions at T_N and T_{OPT} (C) the F and G components of the two magnetic structures of BF-0.25PT above and below T_{OPT}. [after Bhattacharjee et al.(2013)]

There is a significant improvement in the magnetic property of BF-xPT thin film over bulk powder was observed. Hongri et al. have reported that 70 nm thick film of BF-xPT (x= 0.05) exhibits the large value of saturation magnetization of 29.44 emu/ cm^3 [Hongri et al. (2006)]. Gupta et al. also reported that thin film of BF-xPT of thickness between (300-500nm) shows saturated magnetic hysteresis loop. The highest magnetization of ~15 emu/cm^3 is exhibited for the x = 0.27, which indicates the melting of spin spiral in the film of BF-xPT [Gupta et al. (2011)].

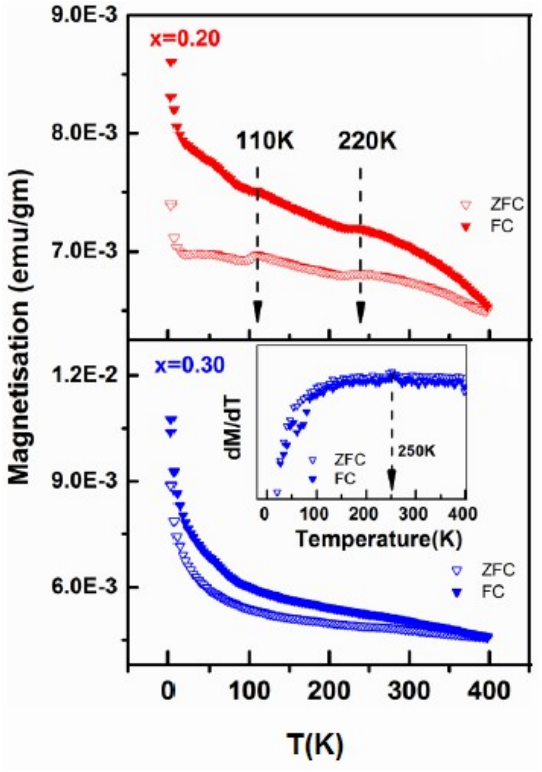

Fig.1.24 Field cooled-zero field cooled (FC-ZFC) magnetization data for BF–xPT (=0.2,0.3) samples [after Katoch et al (2016)].

1.16.3 High temperature studies

BF-xPT solid solution shows interesting thermal expansion properties and coupling between lattice degree of freedom and magnetic. Sai Sundar et al. have studied large change of unit cell parameters over a very narrow temperature range near the ferroelectric transition temperature in the tetragonal phase [Sai Sundar et al. (1995)]. This thermal expansion behavior in tetragonal phase is reported by [Chen et al. (2006)], in which the thermal expansion behavior of the tetragonal phases are studied by using high temperature neutron powder diffraction. The temperature variations of lattice parameters as observed by Chen et al. are shown in Fig. 1.25(a & b). Ranjan et al. have also carried out high temperature x-ray diffraction studies in the tetragonal compositions of BF-xPT [Ranjan et al (2010)]. Variations of lattice parameters as reported by Ranjan et al have shown in Fig1.26. Kothai et al. have reported, using neutron powder diffraction study, that BF-0.35PT shows different structural transitions between cubic, tetragonal and rhombohedral. The details of transitions are given in fig.1.27 [Kothai et al. (2013)].

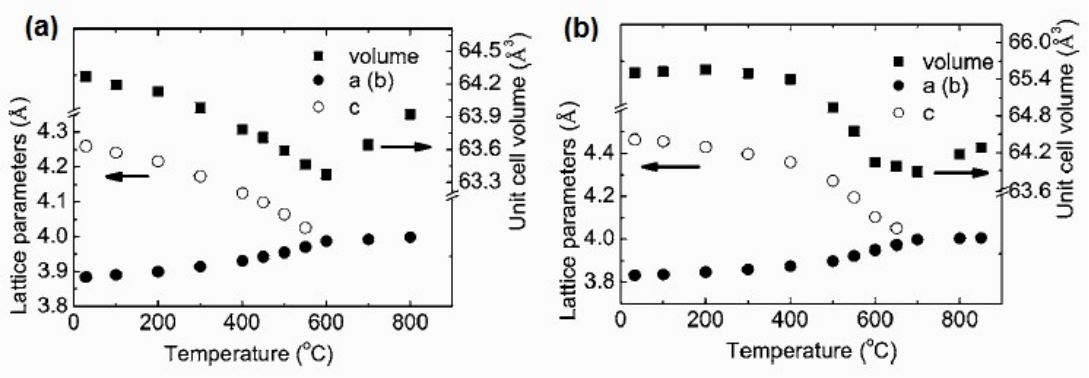

Fig .1.25 (a) Variation of lattice parameters and cell volume of (a) $0.7PbTiO_3$–$0.3BiFeO_3$ and (b) $0.4PbTiO_3$–$0.6BiFeO_3$ [Chen et al. (2006)].

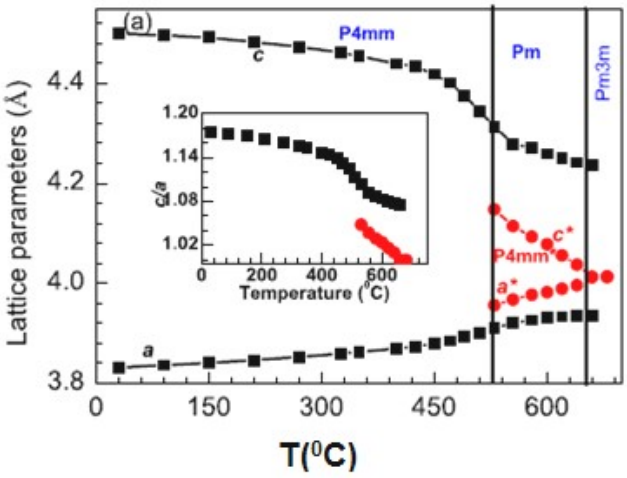

Fig. 1.26 Variation of lattice parameters with temperature [Ranjan et al (2010)]

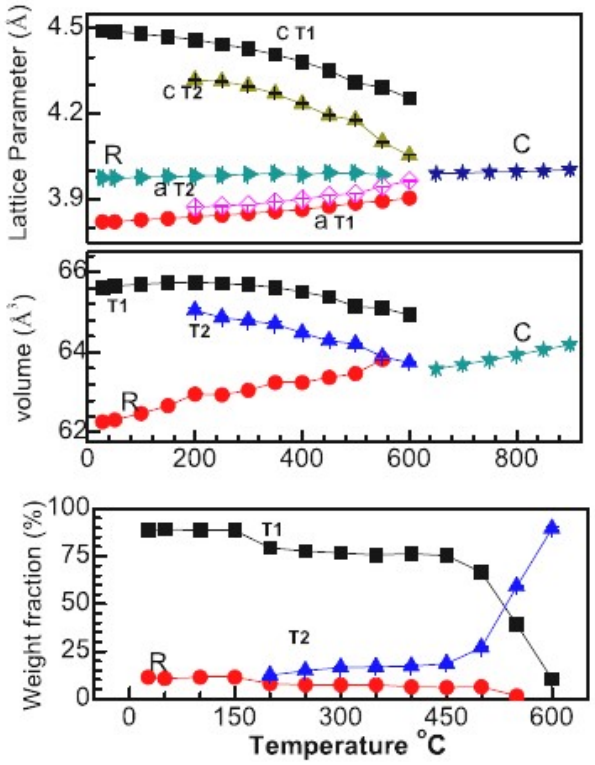

Fig.1.27 Variation of the lattice parameter, cell volume and volume fraction of T1 (tetragonal), T2 (tetragonal) and R (rhombohedral) phases obtained from Rietveld refinement [Kothai et al.(2013)].

1.17 Objective of the Present Thesis

In the previous study we have observed that with decreasing particle size, the suppression of the spiral spin structure increases, which play crucial role to improve the magnetic property of $BiFeO_3$. These nano-structured multiferroic systems provide new possibilities in development of net generation devices in the area of actuators, sensors, data storage and new memory systems.

The main objectives of the present work are as follows:

1. To synthesize pure phase of nanocrystalline of $BiFeO_3$-$xPbTiO_3$ (BF-xPT) powder with varying sizes.

2. To study the size dependent structure changes at room temperature for the composition range of $0.2 \leq x \leq 0.5$.

3. To study the size dependent structural and magnetic properties of composition above the MPB by taking the example of BF-0.50PT.

4. To study the size dependent structural and magnetic properties of composition below the MPB by taking the example of BF-0.25PT.

5. Effect of size on the temperature induced isostructural phase transition in the tetragonal phase of BF-xPT.